Applied Physics Letters ARTICLE pubs.aip.org/aip/apl

Resonantly enhanced evaporation sensing in liquid droplet whispering-gallery cavities

Cite as: Appl. Phys. Lett. **127**, 121101 (2025); doi: 10.1063/5.0279509
Submitted: 28 May 2025 · Accepted: 26 August 2025 ·
Published Online: 22 September 2025

Fan Cheng and Tal Carmon[a)]

AFFILIATIONS

School of Electrical Engineering, Tel Aviv University, Tel Aviv 6997801, Israel

[a)]Author to whom correspondence should be addressed: total@tauex.tau.ac.il

ABSTRACT

We experimentally demonstrate resonantly enhanced measurements of droplet evaporation by tracking whispering-gallery-mode resonances. Droplet optical Q-factors exceeding 2×10^8, coupled to a standard optical fiber, enable operation for several days and evaporation measurement as fine as the release of a single-molecular layer every 50 s! We observe that lower viscosities are associated with faster evaporation, since its molecules are shorter and, hence, have weaker cohesive forces per molecule and higher Brownian velocities. To our surprise, long-term measurements resulted in an exponentially decaying evaporation rate, explained by the early evaporation of shorter molecules, leaving a majority of longer molecules possessing lower vapor pressure.

Whispering-gallery mode (WGM) resonators play a major role in detection[1–9] in fields ranging from biology[10–12] and chemistry[13] to environmental[14,15] and nanoparticle sensing.[16–18] In biology, WGM resonators were used for monitoring cardiac tissues[19–21] and biointerfaces,[22,23] detecting single virus,[24–26] nano-particles,[27,28] DNA,[29,30] and protein molecules.[31–33] Such WGM sensors rely on submerged dielectric spheres[34,35] and toroids[36,37] as well as on liquid filled bottles.[38–42] In these resonators, the solid–liquid interface acts as the cavity wall. A different type of WGM sensor relies on a droplet *per se*.[43–48] In such droplet configurations, the walls of the droplets are made of gas–liquid[49–55] or liquid–liquid[56–58] (e.g., water–oil) interface. As such, the droplet's surface is free to move. These droplets were used to sense Brownian[54]- and induced[59]-capillary oscillations, temperature,[57,60] and humidity[44,61] as well as to function as continuous in time lasers.[46] Positioning control of such droplets relative to a tapered fiber coupler was demonstrated via optical tweezing the droplet in both air[43] and water[48] environments.

For evaporation measurements, tweezed droplets were monitored via free space coupling for their Mie[62–64] scattering and Fano combs.[63] Here, we employ a similar principle—tracking changes in optical resonance as the droplet radius evolves—but without using optical tweezers, which can heat the droplet and affect its evaporation dynamics. Instead, we utilize high-quality-factor optical modes and couple light into and out of the droplet via a standard optical fiber. In detail, by converting the measured resonant wavelength shifts into radius changes, we monitor evaporation rates. Special attention is given to monitor changes in evaporation rates over long times and to different viscosities (5, 10, and 20 cSt).

The evaporation behavior of liquids is fundamentally linked to their molecular structure.[65,66] For example, low-viscosity silicone oils consist of shorter polymer chains with lower molecular weights, which experience weaker intermolecular attractions and possess higher average molecular speeds, leading to faster evaporation. In contrast, high-viscosity oils, composed of longer polymer chains, exhibit stronger intermolecular attractions and lower average molecular speeds, therefore evaporate more slowly. Low evaporation rates correspond to low vapor pressure and vice versa. A detailed thermodynamic description of evaporation can be found in Ref. 67.

As oil evaporates, the shorter, faster, and less cohesive molecules escape first. Over time, primarily longer molecules remain; these molecules volatilize much more slowly. As a result, the overall rate declines and eventually approaches a very low value, a phenomenon termed evaporation saturation.[68,69] This saturation differs from cases in which nonvolatile solutes, such as salts, are left behind after the solvent evaporates.

In our experimental setup, as illustrated in Fig. 1(a), a 970 nm laser (New Focus, TLB-6700) is coupled into a tapered optical fiber,[70,71] with the transmitted signal detected on the other side of the tapered fiber, by a photodetector (New Focus, 1801). The output signal is monitored in real time using an oscilloscope, allowing observation of

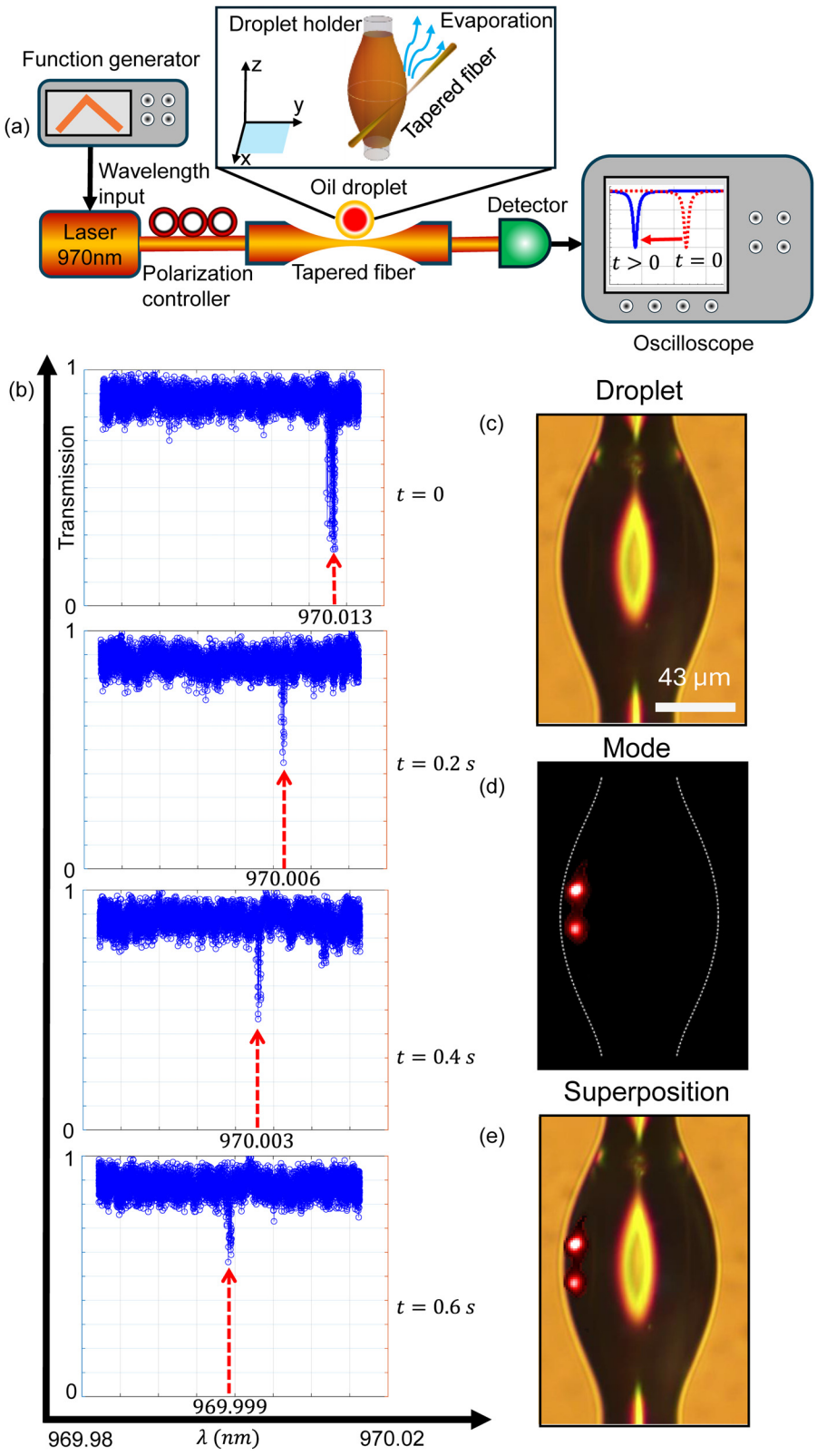

FIG. 1. Experimental setup where (a) droplet evaporation is measured via the (b) continuous drift in the droplet transmission spectrum. The plots represent a 0.02 nm/s change in droplet radius corresponding to the evaporation of a single-molecular layer every 5 s. A supplementary video includes a film of such a drifting resonance (see also supplementary material Note 1). (c) Micrograph of a typical droplet. (d) A cross-sectional profile of a typical optical mode acquired using a NIR camera through residual forward Rayleigh scattering. (e) A superposition of the two preceding micrographs. Multimedia available online.

the resonance wavelength shifts caused by droplet evaporation. A function generator is employed to repeatedly scan the laser wavelength while passing through the drifting resonances. A polarization controller is used to manipulate the polarization state within the fiber, thereby improving the coupling efficiency for one of the polarizations. To prepare the droplet, a conical fiber tip is dipped into a small volume of silicone oil (XIAMETER; viscosity: 5/10/20 cSt; refractive index: 1.396/1.3989/1.4009), forming a liquid optical resonator. The balance between surface tension and gravity enables the stable attachment of a single silicone oil droplet at the fiber tip, as shown in the 3D subpanel of Fig. 1(a). The droplet moves along the vertical cone, mainly in the axial direction, and stops at a position where the combined energies of gravity, liquid–air surface tension, and liquid–solid surface tension reach a minimum. The fiber tip is mounted (vertically) on a precision translation stage (PI; microtranslation stage: M-105; nanopositioner: P-611.3), allowing for fine positioning control of the tapered coupler in the non-contact regime relative to the droplet.

During the experiment, the liquid resonator continuously evaporates into the air, as illustrated by the blue arrows in Fig. 1(a), leading to a gradual decrease in its diameter. We continuously monitor the droplet's diameter via the drifting resonance-wavelength, $\lambda_0(t)$, as described by

$$M\frac{\lambda_0(t)}{n} = 2\pi R(t), \tag{1}$$

where M is the integer corresponding to the number of wavelengths, resonating along the circumference of the droplet, n is the refractive index of the resonator, and R is the radius of the resonator.

Figure 1(b) (Multimedia view) illustrates the temporal evolution of the resonance wavelength of the droplet resonator (10 cSt). The x axis represents the resonance wavelength in vacuum, while the y axis denotes the normalized transmission. Four subfigures are displayed sequentially from top to bottom, corresponding to time points between 0 and 0.6 s. Over this 0.6 s interval, the resonance wavelength exhibits a blue shift of 0.014 nm, corresponding to a shift rate of approximately 0.02 nm/s. Bearing in mind that the Bohr diameter of an atom is approximately 0.1 nm, the measured evaporation rate of 0.02 nm/s corresponds to the release of a single-molecular layer (give or take) into the air every 5 s. In what follows, even lower evaporation rates were observed, corresponding to the evaporation of a single-molecular layer every 50 s. The detailed tracking method for moving resonance peaks can be found in supplementary material Note 2.

While Fig. 1(b) captures the temporal evolution of the resonance wavelength, Figs. 1(c)–1(e) provide spatial information about the droplet resonator and the confined optical mode. Specifically, Fig. 1(c) shows a micrograph of a typical droplet, Fig. 1(d) presents the cross-sectional profile of a typical optical mode captured using a NIR camera through residual forward Rayleigh scattering, and Fig. 1(e) displays a superposition of the two, illustrating the position of the mode within the droplet.

The evaporation dynamics of silicone oil droplets with different viscosities were analyzed by monitoring the resonance wavelength shift over time and converting it into the corresponding radius change using the optical resonance condition. The resonance condition for the droplet resonator can be expressed as

$$\lambda_0(t) = \frac{2\pi n R(t)}{M}, \tag{2}$$

where $\lambda_0(t)$ is the resonance wavelength as a function of time, $R(t)$ is the resonator radius as a function of time, n is the refractive index of the silicone oil (assumed constant), and M is the mode number (assumed constant). Here, $R(t)$ is further expressed as

$$R(t) = R_0 + \Delta R(t), \tag{3}$$

where R_0 denotes the droplet radius at equilibrium and $\Delta R(t)$ represents the deviation from the equilibrium position due to evaporation. Based on this relationship, the time-dependent radius change $\Delta R(t)$ was extracted from the measured $\lambda_0(t)$.

Figure 2 presents the normalized radius change, $\Delta R(t)$, as a function of time for three types of silicone oil with viscosities of 5, 10, and 20 cSt. Linear fitting was applied to each dataset to determine the radius change rates, expressed in nm/s. The fitted rates are −13.1 nm/s for 5 cSt (Droplet diameter: 151.2 μm), −1.3 nm/s for 10 cSt (Droplet diameter: 129.8 μm), and −0.1 nm/s for 20 cSt (Droplet diameter: 116.9 μm). To give a scale, the later evaporation rate corresponds to the evaporation of a single-molecular layer every 50 s. The 5, 10, and 20 cSt measurements were conducted immediately after droplet formation. The results demonstrate that droplets with lower viscosity exhibit faster radius reduction, as indicated by the steeper slopes.

To investigate the long-term evaporation dynamics, a 5 cSt silicone oil droplet resonator was repeatedly measured over a 22 h period. Figure 3 shows the time evolution of the radius and the corresponding evaporation rate, defined as $-\dot{R}(t)$. The radius change rate ($\dot{R}(t)$) as a function of time is presented in Fig. 3(a). The experimentally measured evaporation rate, $-\dot{R}(t)$, was fitted with a single-exponential decay function of the form

$$\dot{R}(t) = \dot{R}_0 e^{-\frac{t}{\tau}}, \tag{4}$$

where $\dot{R}_0$ is the initial evaporation rate and τ is the evaporation-saturation time constant. Best fitting Eq. (4) to our experimental result gave a time constant of 0.6 h and initial evaporation rate of 12.8 nm/s. We note that the refraction index also changes during evaporation.[72] However, refraction changes account for less than 0.4% of the optical path length variation. This is in comparison to 37.9% changes in droplet radius.

Liquid droplets extend the capacities of solid-based devices by being a million times softer than comparable solid structures, making

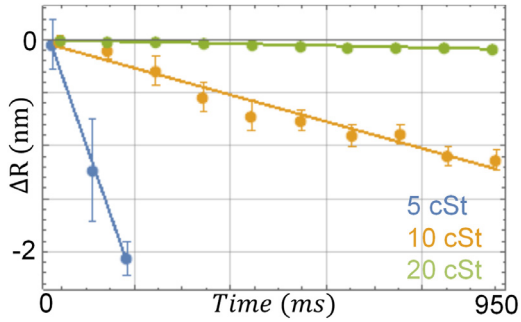

FIG. 2. Droplet radius vs Time is derived from the resonance wavelength shift using the optical resonance condition. Solid lines represent linear fits to the experimental data. The extracted radius change rates are −13.1 nm/s for 5 cSt (Droplet diameter: 151.2 μm), −1.3 nm/s for 10 cSt (Droplet diameter: 129.8 μm), and −0.1 nm/s for 20 cSt (Droplet diameter: 116.9 μm). The 5, 10, and 20 cSt measurements were conducted immediately after preparation.

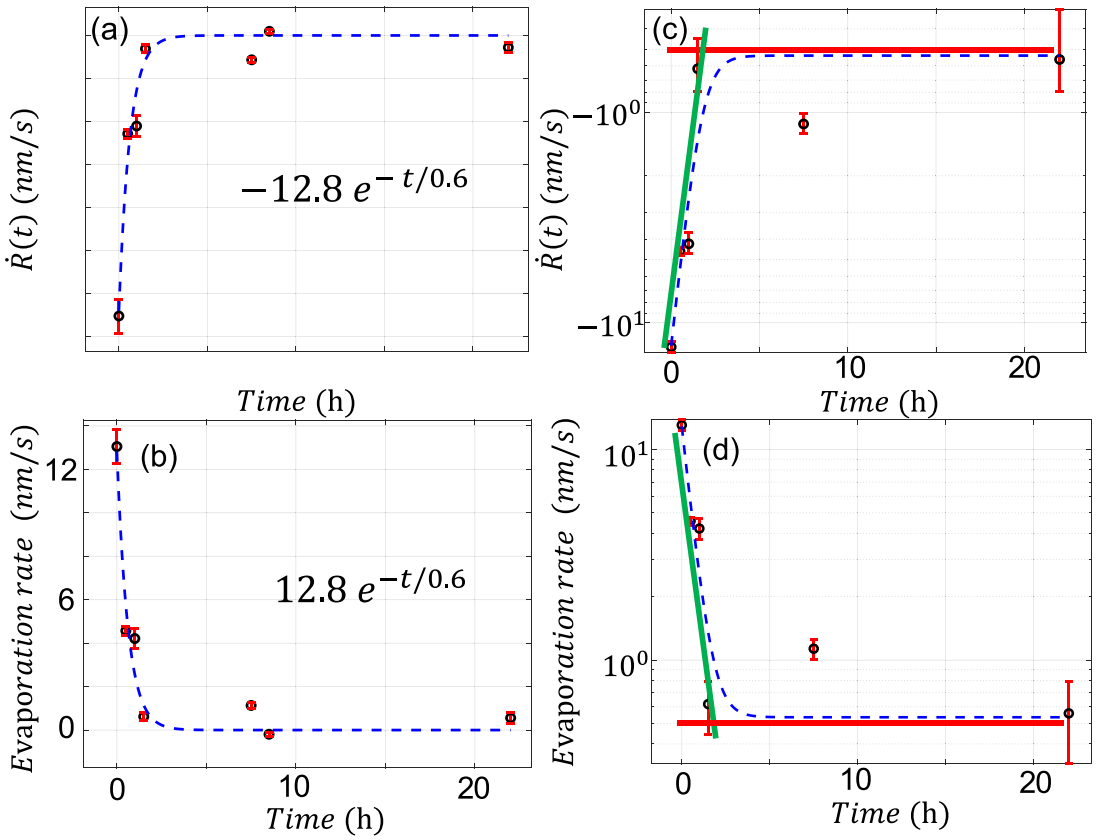

FIG. 3. Time evolution of the radius change rate ($\dot{R}(t)$) and evaporation rate ($-\dot{R}(t)$) of a 5 cSt silicone oil droplet resonator over a 22 h period. (a) Radius change rate ($\dot{R}(t)$) as a function of time, fitted to theory. The error bars correspond to the standard deviation of the radius change rate, obtained from the linear fitting in Fig. 2. (b) Evaporation rate, defined as $-\dot{R}(t)$, following an exponential decay with the same fitting form. (c) and (d) Same data as in (a) and (b), respectively, but plotted with a logarithmic y axis to highlight the exponential decay behavior.

them correspondingly more sensitive to external forces. Furthermore, the droplet's liquid-phase boundary can absorb or repel particles based on surface tension considerations. Additionally, components in the liquid can evaporate into the surroundings, and surrounding components can be absorbed by the liquid. Going to such new frontiers requires a consideration of evaporation as we measure here. Our drifting resonance tracking might impact droplet microfluidics by performing experiments using a tunable laser with a properly wideband that can track a single resonance throughout the experiment time. Alternatively, a short-band tunable laser can monitor a set of resonances, while new resonances replace those drifting out. Another insight relates to the properties of oils. An oil with specific viscosity can be prepared in two ways: (1) mixing low-viscosity and high-viscosity oil where the polymer chains are identical in chemical composition but differ in length, and (2) using oil where all molecules are of the same length, give or take. While these two options are identical when working in an enclosed vessel, this is not the case when exposed to air. In this latter case, the oil mixture will increase its viscosity over time, while the constant-length molecules will not.

See the supplementary material for the multimedia available online and the tracking method for moving resonance dips.

This work was supported by the United States-Israel Binational Science Foundation (NSF-BSF) (2020683) and Israeli Science Foundation (537/20). We would like to thank Anat Korek (Brenntag Israel Ltd.) for providing various silicone oils used in this study.

AUTHOR DECLARATIONS

Conflict of Interest

The authors have no conflicts to disclose.

Author Contributions

Fan Cheng: Data curation (lead); Formal analysis (lead); Writing – original draft (lead). **Tal Carmon:** Conceptualization (lead); Funding acquisition (lead); Supervision (lead); Writing – review & editing (lead).

DATA AVAILABILITY

The data that support the findings of this study are available from the corresponding author upon reasonable request.

REFERENCES

[1]X. Fan, I. M. White, S. I. Shopova, H. Zhu, J. D. Suter, and Y. Sun, "Sensitive optical biosensors for unlabeled targets: A review," Anal. Chim. Acta **620**, 8–26 (2008).

[2]F. Vollmer and S. Arnold, "Whispering-gallery-mode biosensing: Label-free detection down to single molecules," Nat. Methods **5**, 591–596 (2008).

[3]S. Soria, S. Berneschi, M. Brenci, F. Cosi, G. Nunzi Conti, S. Pelli, and G. C. Righini, "Optical microspherical resonators for biomedical sensing," Sensors **11**, 785–805 (2011).

[4]M. R. Foreman, J. D. Swaim, and F. Vollmer, "Whispering gallery mode sensors," Adv. Opt. Photonics **7**, 168–240 (2015).

[5]S. Yang, Y. Wang, and H. Sun, "Advances and prospects for whispering gallery mode microcavities," Adv. Opt. Mater. **3**, 1136–1162 (2015).

[6]Y. Zhang, T. Zhou, B. Han, A. Zhang, and Y. Zhao, "Optical bio-chemical sensors based on whispering gallery mode resonators," Nanoscale **10**, 13832–13856 (2018).

[7]X. Jiang, A. J. Qavi, S. H. Huang, and L. Yang, "Whispering-gallery sensors," Matter **3**, 371–392 (2020).

[8]Y. Wang, S. Zeng, G. Humbert, and H.-P. Ho, "Microfluidic whispering gallery mode optical sensors for biological applications," Laser Photonics Rev. **14**, 2000135 (2020).

[9]S. Hao and J. Su, "Whispering gallery mode optical resonators for biological and chemical detection: Current practices, future perspectives, and challenges," Rep. Prog. Phys. **88**, 016402 (2025).

[10]F. Vollmer, D. Braun, A. Libchaber, M. Khoshsima, I. Teraoka, and S. Arnold, "Protein detection by optical shift of a resonant microcavity," Appl. Phys. Lett. **80**, 4057–4059 (2002).

[11]M. Loyez, M. Adolphson, J. Liao, and L. Yang, "From whispering gallery mode resonators to biochemical sensors," ACS Sens. **8**, 2440–2470 (2023).

[12]D. Yu, M. Humar, K. Meserve, R. C. Bailey, S. N. Chormaic, and F. Vollmer, "Whispering-gallery-mode sensors for biological and physical sensing," Nat. Rev. Methods Primer **1**, 83 (2021).

[13]S. H. Huang, S. Sheth, E. Jain, X. Jiang, S. P. Zustiak, and L. Yang, "Whispering gallery mode resonator sensor for in situ measurements of hydrogel gelation," Opt. Express **26**, 51–62 (2018).

[14]Y. Yang, S. Saurabh, J. M. Ward, and S. N. Chormaic, "High-Q, ultrathin-walled microbubble resonator for aerostatic pressure sensing," Opt. Express **24**, 294–299 (2016).

[15]X. Xu, W. Chen, G. Zhao, Y. Li, C. Lu, and L. Yang, "Wireless whispering-gallery-mode sensor for thermal sensing and aerial mapping," Light **7**, 62 (2018).

[16]S. Arnold, D. Keng, S. I. Shopova, S. Holler, W. Zurawsky, and F. Vollmer, "Whispering gallery mode carousel – A photonic mechanism for enhanced nanoparticle detection in biosensing," Opt. Express **17**, 6230–6238 (2009).

[17]J. Zhu, S. K. Ozdemir, Y.-F. Xiao, L. Li, L. He, D.-R. Chen, and L. Yang, "On-chip single nanoparticle detection and sizing by mode splitting in an ultrahigh-Q microresonator," Nat. Photonics **4**, 46–49 (2010).

[18]J. M. Ward, Y. Yang, F. Lei, X.-C. Yu, Y.-F. Xiao, and S. N. Chormaic, "Nanoparticle sensing beyond evanescent field interaction with a quasi-droplet microcavity," Optica **5**, 674 (2018).

[19]A. Chaichi, A. Prasad, and M. R. Gartia, "Raman spectroscopy and microscopy applications in cardiovascular diseases: From molecules to organs," Biosensors **8**, 107 (2018).

[20]M. Schubert, L. Woolfson, I. R. M. Barnard, A. M. Dorward, B. Casement, A. Morton, G. B. Robertson, P. L. Appleton, G. B. Miles, C. S. Tucker, S. J. Pitt, and M. C. Gather, "Monitoring contractility in cardiac tissue with cellular resolution using biointegrated microlasers," Nat. Photonics **14**, 452–458 (2020).

[21]H. Kavand, R. Nasiri, and A. Herland, "Advanced materials and sensors for microphysiological systems: Focus on electronic and electrooptical interfaces," Adv. Mater. **34**, 2107876 (2022).

[22]Z. Wang, Y. Zhang, X. Gong, Z. Yuan, S. Feng, T. Xu, T. Liu, and Y.-C. Chen, "Bio-electrostatic sensitive droplet lasers for molecular detection," Nanoscale Adv. **2**, 2713–2719 (2020).

[23]Y. Fu, S. Lin, and X.-H. Wang, "Whispering gallery mode micro/nanolasers for intracellular probing at single cell resolution," ACS Sens. **9**, 5683–5698 (2024).

[24]V. R. Dantham, S. Holler, V. Kolchenko, Z. Wan, and S. Arnold, "Taking whispering gallery-mode single virus detection and sizing to the limit," Appl. Phys. Lett. **101**, 043704 (2012).

[25]J. G. Zhu, S. K. Ozdemir, L. He, D. R. Chen, and L. Yang, "Single virus and nanoparticle size spectrometry by whispering-gallery-mode microcavities," Opt. Express **19**, 16195–16206 (2011).

[26]L. N. He, K. Ozdemir, J. G. Zhu, W. Kim, and L. Yang, "Detecting single viruses and nanoparticles using whispering gallery microlasers," Nat. Nanotechnol. **6**, 428–432 (2011).

[27]Y. Hu, L. Shao, S. Arnold, Y.-C. Liu, C.-Y. Ma, and Y.-F. Xiao, "Mode broadening induced by nanoparticles in an optical whispering-gallery microcavity," Phys. Rev. A **90**, 043847 (2014).

[28]M. R. Foreman, D. Keng, E. Treasurer, J. R. Lopez, and S. Arnold, "Whispering gallery mode single nanoparticle detection and sizing: The validity of the dipole approximation," Opt. Lett. **42**, 963–966 (2017).

[29]S. Panich, M. Haj Sleiman, I. Steer, S. Ladame, and J. B. Edel, "Real-time monitoring of ligand binding to G-quadruplex and duplex DNA by whispering gallery mode sensing," ACS Sens. **1**, 1097–1102 (2016).

[30]X. Zhou, S. Wang, X. Li, Y. Zhao, Y. Zhang, L. V. Nguyen, and S. C. Warren-Smith, "Whispering gallery mode microresonator sensor integrated in exposed core fiber for label-free DNA hybridization detection," J. Lightwave Technol. **41**, 4502–4508 (2023).

[31]M. Noto, D. Keng, I. Teraoka, and S. Arnold, "Detection of protein orientation on the silica microsphere surface using transverse electric/transverse magnetic whispering gallery modes," Biophys. J. **92**, 4466–4472 (2007).

[32]C. E. Soteropulos, K. M. Zurick, M. T. Bernards, and H. K. Hunt, "Tailoring the protein adsorption properties of whispering gallery mode optical biosensors," Langmuir **28**, 15743–15750 (2012).

[33]A. Jonáš, M. Aas, Y. Karadag, S. Manioğlu, S. Anand, D. McGloin, H. Bayraktar, and A. Kiraz, "*In vitro* and *in vivo* biolasing of fluorescent proteins suspended in liquid microdroplet cavities," Lab Chip **14**, 3093–3100 (2014).

[34]N. M. Hanumegowda, C. J. Stica, B. C. Patel, I. White, and X. Fan, "Refractometric sensors based on microsphere resonators," Appl. Phys. Lett. **87**, 201107 (2005).

[35]W. Kim, S. K. Ozdemir, J. Zhu, and L. Yang, "Observation and characterization of mode splitting in microsphere resonators in aquatic environment," Appl. Phys. Lett. **98**, 141106 (2011).

[36]W. Kim, S. K. Ozdemir, J. Zhu, L. He, and L. Yang, "Demonstration of mode splitting in an optical microcavity in aqueous environment," Appl. Phys. Lett. **97**, 71111 (2010).

[37]W. Kim, S. K. Ozdemir, J. Zhu, F. Monifi, C. Coban, and L. Yang, "Detection and size measurement of individual hemozoin nanocrystals in aquatic environment using a whispering gallery mode resonator," Opt. Express **20**, 29426–29446 (2012).

[38]I. M. White, H. Oveys, and X. Fan, "Liquid-core optical ring-resonator sensors," Opt. Lett. **31**, 1319–1321 (2006).

[39]M. Sumetsky, Y. Dulashko, and R. S. Windeler, "Optical microbubble resonator," Opt. Lett. **35**, 898–900 (2010).

[40]A. Watkins, J. Ward, Y. Wu, and S. Nic Chormaic, "Single-input spherical microbubble resonator," Opt. Lett. **36**, 2113–2115 (2011).

[41]W. Lee, Y. Sun, H. Li, K. Reddy, M. Sumetsky, and X. Fan, "A quasi-droplet optofluidic ring resonator laser using a micro-bubble," Appl. Phys. Lett. **99**, 091102 (2011).

[42]K. H. Kim, G. Bahl, W. Lee, J. Liu, M. Tomes, X. Fan, and T. Carmon, "Cavity optomechanics on a microfluidic resonator with water and viscous liquids," Light **2**, e110 (2013).

[43]S. Kaminski, L. L. Martin, and T. Carmon, "Tweezers controlled resonator," Opt. Express **23**, 28914–28919 (2015).

[44]L. Labrador-Páez, K. Soler-Carracedo, M. Hernández-Rodríguez, I. R. Martín, T. Carmon, and L. L. Martin, "Liquid whispering-gallery-mode resonator as a humidity sensor," Opt. Express **25**, 1165 (2017).

[45]A. Giorgini, S. Avino, P. Malara, P. De Natale, M. Yannai, T. Carmon, and G. Gagliardi, "Stimulated Brillouin cavity optomechanics in liquid droplets," Phys. Rev. Lett. **120**, 073902 (2018).

[46]S. Maayani and T. Carmon, "Droplet Raman laser coupled to a standard fiber," Photonics Res. **7**, 1188 (2019).

[47]A. Giorgini, S. Avino, P. Malara, P. De Natale, and G. Gagliardi, "Liquid droplet microresonators," Sensors **19**, 473 (2019).
[48]J. Kher-Alden, S. Maayani, L. L. Martin, M. Douvidzon, L. Deych, and T. Carmon, "Microspheres with atomic-scale tolerances generate hyperdegeneracy," Phys. Rev. X **10**, 031049 (2020).
[49]A. Kiraz, A. Kurt, M. A. Dündar, and A. L. Demirel, "Simple largely tunable optical microcavity," Appl. Phys. Lett. **89**, 081118 (2006).
[50]A. Jonáš, Y. Karadag, M. Mestre, and A. Kiraz, "Probing of ultrahigh optical Q-factors of individual liquid microdroplets on superhydrophobic surfaces using tapered optical fiber waveguides," J. Opt. Soc. Am. B **29**, 3240–3247 (2012).
[51]V. D. Ta, R. Chen, and H. D. Sun, "Tuning whispering gallery mode lasing from self-assembled polymer droplets," Sci. Rep. **3**, 1362 (2013).
[52]S. Avino, A. Krause, R. Zullo, A. Giorgini, P. Malara, P. De Natale, H. P. Loock, and G. Gagliardi, "Direct sensing in liquids using whispering-gallery-mode droplet resonators," Adv. Opt. Mater. **2**, 1155–1159 (2014).
[53]S. M. Wildgen and R. C. Dunn, "Whispering gallery mode resonators for rapid label-free biosensing in small volume droplets," Biosensors **5**, 118–130 (2015).
[54]S. Maayani, L. L. Martin, S. Kaminski, and T. Carmon, "Cavity optocapillaries," Optica **3**, 552–555 (2016).
[55]S. Maayani, L. L. Martin, and T. Carmon, "Water-walled microfluidics for high-optical finesse cavities," Nat. Commun. **7**, 10435 (2016).
[56]S. Anand, M. Eryürek, Y. Karadag, A. Erten, A. Serpengüzel, A. Jonáš, and A. Kiraz, "Observation of whispering gallery modes in elastic light scattering from microdroplets optically trapped in a microfluidic channel," J. Opt. Soc. Am. B **33**, 1349–1354 (2016).
[57]Z. Liu, L. Liu, Z. Zhu, Y. Zhang, Y. Wei, X. Zhang, E. Zhao, Y. Zhang, J. Yang, and L. Yuan, "Whispering gallery mode temperature sensor of liquid microresonastor," Opt. Lett. **41**, 4649–4652 (2016).
[58]F. Cheng, V. Shuvayev, M. Douvidzon, L. Deych, and T. Carmon, "Cavity continuum," Photonics Res. **12**, 391–398 (2024).
[59]S. Kaminski, L. L. Martin, S. Maayani, and T. Carmon, "Ripplon laser through stimulated emission mediated by water waves," Nat. Photonics **10**, 758–761 (2016).
[60]Y. Wang, H. Li, L. Zhao, Y. Liu, S. Liu, and J. Yang, "Tapered optical fiber waveguide coupling to whispering gallery modes of liquid crystal microdroplet for thermal sensing application," Opt. Express **25**, 918–926 (2017).
[61]P. K. Reinis, L. Milgrave, K. Draguns, I. Brice, J. Alnis, and A. Atvars, "High-sensitivity whispering gallery mode humidity sensor based on glycerol microdroplet volumetric expansion," Sensors **21**, 1746 (2021).
[62]M. Kolwas, D. Jakubczyk, G. Derkachov, and K. Kolwas, "Interaction of optical whispering gallery modes with the surface layer of evaporating droplet of suspension," J. Quant. Spectrosc. Radiat. Transf. **131**, 138–145 (2013).
[63]J. T. Marmolejo, A. Canales, D. Hanstorp, and R. Méndez-Fragoso, "Fano combs in the directional Mie scattering of a water droplet," Phys. Rev. Lett. **130**, 043804 (2023).
[64]S. M. Iftiquar, "Observing variation in whispering gallery mode resonance of a trapped and levitated dye doped microdrop," J. Fluoresc. **35**, 2895 (2024).
[65]M. F. Fingas, "Studies on the evaporation of crude oil and petroleum products: I. the relationship between evaporation rate and time," J. Hazard. Mater. **56**, 227–236 (1997).
[66]W. L. H. Hallett and N. A. Clark, "A model for the evaporation of biomass pyrolysis oil droplets," Fuel **85**, 532–544 (2006).
[67]D. N. Gerasimov and E. I. Yurin, *Kinetics of Evaporation* (Springer International Publishing, 2018), Vol. 68.
[68]R. R. Buch and A. R. Huntress, "Organosiloxane working fluids for the liquid droplet radiator," Report No. NASA-CR-175033, 1985.
[69]Z. Wang, D. Orejon, Y. Takata, and K. Sefiane, "Wetting and evaporation of multicomponent droplets," Phys. Rep. **960**, 1–37 (2022).
[70]J. C. Knight, G. Cheung, F. Jacques, and T. A. Birks, "Phase-matched excitation of whispering-gallery-mode resonances by a fiber taper," Opt. Lett. **22**, 1129 (1997).
[71]M. Cai and K. Vahala, "Highly efficient optical power transfer to whispering-gallery modes by use of a symmetrical dual-coupling configuration," Opt. Lett. **25**, 260–262 (2000).
[72]M. Izdebski, R. Ledzion, and S. Węgrzynowski, "Extremely weak electro-optic Kerr effect in methyl silicone oils," Materials **17**, 1850 (2024).